# IRS-Aided Massive MIMO ISAC Systems

Ranga Kulathunga, Janith Kavindu Dassanayake, and Gayan Amarasuriya
School of Electrical, Computer, and Biomedical Engineering, Southern Illinois University, Carbondale, IL, USA 62901
Email: {ranga.kulathunga, janith.dassanayake, gayan.baduge}@siu.edu

***Abstract*—The performance of integrated sensing and communications (ISAC) empowered intelligent reflecting surface (IRS)-aided massive multiple-input multiple-output (MIMO) systems operating over spatially correlated Rician fading is investigated. Computationally-efficient linear precoders are used to construct the ISAC signal by invoking the maximal ratio transmission (MRT) criterion into the composite channels containing both direct and IRS reflected channels. The uplink communication channels are estimated based on the linear minimum mean square error criterion and used to construct user precoders. The IRS phase-shifts are optimized based on the statistical channel knowledge to maximize the minimum average power gains of the composite communication channels subject to an average power threshold for the reflected sensing channel. The communication performance is evaluated by deriving the achievable user rates, while the sensing performance is studies by locating the target via the 2D MUltiple SIgnal Classification (MUSIC) algorithm. Our numerical results are used to study the trade-off between the communication and sensing performance metrics in IRS-aided massive MIMO systems with MRT-based linear precoders.**

## I. Introduction

The sixth-generation (6G) wireless is expected to support wide-range services, including autonomous driving, industrial automation, environmental sensing, and extended reality [1]. Such 6G use-cases necessitate precise sensing in addition to high rate reliable communications [2]. However, the sensing and communications services are currently being rendered in separate hardware units. Integrated sensing and communications (ISAC) has recently been envisioned to deliver both sensing and communication functionalities within the same hardware unit by using the same spectrum [2]. Thus, ISAC can be leveraged to boost energy, spectral, and cost efficiency aiming to meet the key performance indicators of 6G and beyond [2]. Novel ISAC system models are currently being designed by innovating joint waveforms, beamformers, estimators, detectors, and localizers [2]–[7].

On one hand, massive multiple-input-multiple-output (MIMO) has been one of the foundational pillars of the fifth-generation (5G) wireless. It leverages large degrees-of-freedom and array gains rendered by massive antenna arrays at the base-station (BS) to render huge spatial multiplexing and energy efficiency gains [8]. The channel hardening and favorable propagation of massive MIMO have been exploited to theoretically prove that simple linear precoders designed based on maximal ratio transmission (MRT) principle can operate near-optimally in the large antenna regime [8].

On the other hand, intelligent reflecting surfaces (IRSs) have emerged as a pivotal technology that can be leveraged to smartly control wireless propagation. An IRS consists of a large number of tiny reflecting elements capable of introducing passive phase-shifts into the electromagnetic waves impinging upon them [9]. These IRS elements are made out of meta-materials, and hence, it provides a cost-effective viable solutions to boost the end-to-end reliability and coverage. A myriad of joint precoder and phase-shift optimization techniques have been developed (see [9] and references therein).

The potentials of IRS-aided massive MIMO can be leveraged to boost ISAC performance. The research on IRS-aided massive MIMO ISAC is still at an its infancy [3]–[7]. In [3], the transmit waveform and IRS phase-shifts have been optimized to maximize the signal-to-interference-plus-noise ratio (SINR) for radar detection, while delivering quality-of-service (QoS) constraints for the communication users via alternative direction method of multipliers (ADMM) and majorization-minimization (MM) methods. In [5], the BS precoder and active IRS reflection coefficients have been jointly optimized via MM techniques to maximize SINR for radar while satisfying communication QoS requirements. In [4], a joint waveform and passive precoder design has been proposed by maximizing the SINR for sensing, while minimizing the multi-user interference for communications. In [7], an omni RIS-aided ISAC system has been studied by maximizing the minimum SINR for multi-target sensing, while ensuring a minimum rate threshold for the multiple users via semi-definite relaxation (SDR) and successive convex approximation (SCA). In [6], a transceiver and radar detector optimization framework has been proposed by designing BS precoders and optimizing RIS phase-shifts based on ADMM techniques.

**Motivation and our contribution:** The existing research [3]–[7] on IRS-aided ISAC has aimed to design near-optimal BS precoders and IRS phase-shift matrices via ADMM, MM, SDR, and SCA optimization techniques. However, such designs may result in non-linear precoders, and hence, their computational complexity may become prohibitively complicated for massive MIMO. Simple linear precoders based on MRT principle are appealing to massive MIMO due to their simple implementation [8]. A fundamental performance analysis for IRS-aided massive MIMO ISAC with linear precoders has not yet been reported to the best of our knowledge. Having been motivated by this gap, we present such a performance analysis by considering a practical spatially correlated Rician communication channel model, imperfectly estimated composite channel state information (CSI) via linear mean square error (LMMSE) techniques, and linear precoders designed by applying the MRT principle to the composite channels. The achievable user rates are derived in closed-form, and the target is localized by invoking the 2D MUltiple SIgnal Classification (MUSIC) algorithm. The IRS phase-shifts are optimized based on statistical CSI to maximize the average channel power gain of the weakest user, while meeting a minimum average sensing channel power gain constraint. Our analysis reveal that the IRS-aided massive MIMO with simple linear precoders can be used to fine-tune fundamental ISAC design trade-offs.

ICC 2025 - IEEE International Conference on Communications | 979-8-3315-0521-9/25/$31.00 ©2025 IEEE | DOI: 10.1109/ICC52391.2025.11161470

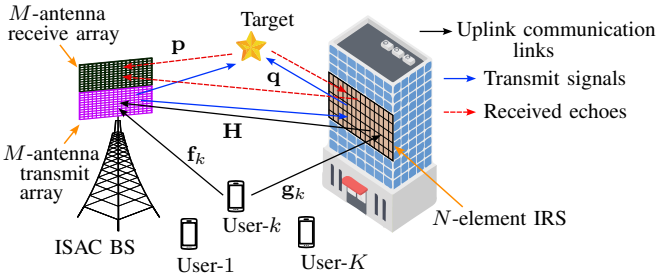


Fig. 1. A system model for enabling ISAC in IRS-aided massive MIMO.

## II. System, Channel and Signal Models

### A. System Model

We consider an IRS-aided massive MIMO ISAC system in which a BS serves $K$ single-antenna users while sensing a target (see Fig. 1). The BS consists of transmit/receive antenna arrays each having $M$ antennas arranged to form a uniform planer array (UPA) with $M_1$ rows and $M_2$ columns satisfying $M_1 \times M_2 = M$. The IRS has a UPA of $N$ passive reflective elements with $N_1$ rows and $N_2$ columns satisfying $N_1 \times N_2 = N$. The $k$th user is denoted by $\mathrm{U}_k$, where $k \in \{1, \cdots, K\}$, and the target is denoted by T.

### B. Communication Channel Model

The IRS-BS, $\mathrm{U}_k$-BS, and $\mathrm{U}_k$-IRS channels are denoted by $\mathbf{H} \in \mathbb{C}^{M \times N}$, $\mathbf{f}_k \in \mathbb{C}^M$, and $\mathbf{g}_k \in \mathbb{C}^N$, respectively. The antennas of BS and IRS are typically installed in towers/rooftops or walls of tall buildings. Hence, the IRS-BS channel consists of a dominant/deterministic line-of-sight (LoS) component in addition to the random non-LoS (NLoS) multi-path components, and it is modeled via spatially correlated Rician fading. Since the channels associated within an IRS set-up is less likely to contain LoS components, $\mathrm{U}_k$-BS and $\mathrm{U}_k$-IRS channels are modeled via spatially correlated Rayleigh fading. Thereby, the channels $\mathbf{H}$, $\mathbf{f}_k$, and $\mathbf{g}_k$ can be modeled as

$$\mathbf{H} = \sqrt{K_H \zeta_H/(K_H+1)}\bar{\bar{\mathbf{H}}} + \sqrt{\zeta_H/(K_H+1)}\mathbf{R}_B^{\frac{1}{2}}\tilde{\mathbf{H}}\mathbf{R}_I^{\frac{1}{2}}, \quad (1)$$

$$\mathbf{f}_k \sim \mathcal{CN}(\mathbf{0}, \mathbf{R}_{f_k}) \quad \text{and} \quad \mathbf{g}_k \sim \mathcal{CN}(\mathbf{0}, \mathbf{R}_{g_k}), \quad (2)$$

where $K_H$ and $\zeta_H$ are the Rician factor and large-scale fading coefficient of $\mathbf{H}$, respectively. We denote $\bar{\mathbf{H}} = (K_H/(K_H+1))^{\frac{1}{2}}\zeta_H^{\frac{1}{2}}\bar{\bar{\mathbf{H}}}$ and $\mathbf{R}_T = (1/(K_H+1))\zeta_H\mathbf{R}_B$. The deterministic LoS channel component ($\bar{\bar{\mathbf{H}}}$) in (1) can be modeled as

$$\bar{\bar{\mathbf{H}}} = \mathbf{a}_B(\phi_H, \upsilon_H)\mathbf{a}_I^H(\psi_H, \delta_H), \quad (3)$$

where $\phi_H$ and $\upsilon_H$ are azimuth and elevation angles-of-arrival (AoA) at the BS for the IRS-BS LoS channel, while $\psi_H$ and $\delta_H$ are azimuth and elevation angles-of-departure (AoD) of IRS-BS channel at the IRS. Then, the beam steering vectors $\mathbf{a}_B$ and $\mathbf{a}_I$ can be modeled as [10]

$$\mathbf{a}_z(x,y) = \mathrm{vec}\left(\mathbf{b}_{z1}(x,y), \mathbf{b}_{z2}^H(x,y)\right) \quad \text{for} \quad z \in \{B, I\}, \quad (4)$$

$$\mathbf{b}_{zi}(x,y) = \left[1, \cdots, e^{-jmq_i(x,y)}, \cdots, e^{-j(P_i-1)q_i(x,y)}\right]^T, \quad (5)$$

where $i \in \{1,2\}$, $(x,y) = (\phi_H, \upsilon_H)$ and $P = M$ if $z = B$, and $(x,y) = (\psi_H, \delta_H)$ and $P = N$ if $z = I$. Here, $m \in \{0, \cdots, P_i - 1\}$. Moreover, $q_1(x,y)$ and $q_2(x,y)$ in (5) can be written as $\pi\cos(x)\sin(y)$ and $\pi\sin(x)\sin(y)$, respectively. In (1), $\tilde{\mathbf{H}}$ is modeled as complex Gaussian distributed with zero mean and unit variance: $\tilde{\mathbf{H}} \sim \mathcal{CN}(\mathbf{0}_{M\times N}, \mathbf{I}_M \otimes \mathbf{I}_N)$.

The covariance matrices $\mathbf{R}_B$, $\mathbf{R}_I$, $\mathbf{R}_{f_k}$, and $\mathbf{R}_{g_k}$ in (1)-(2) capture spatially correlated fading. In (1), $\mathbf{R}_B$ and $\mathbf{R}_I$ are covariance matrices at the BS and IRS, respectively. In (2), $\mathbf{R}_{f_k}$ and $\mathbf{R}_{g_k}$ can be written as $\zeta_{f_k}\mathbf{R}_B$ and $\zeta_{g_k}\mathbf{R}_I$, where $\zeta_{f_k}$ and $\zeta_{g_k}$ are the large-scale fading coefficients of $\mathbf{f_k}$ and $\mathbf{g_k}$, respectively. Then, $\mathbf{R}_B$ and $\mathbf{R}_I$ can be modeled as $\mathbf{R}_z = A_z\tilde{\mathbf{R}}_z$ for $z \in \{B, I\}$ in which the $(i,j)$ element of $\tilde{\mathbf{R}}_z$ can be modeled by using the correlation model for UPAs in [11, Eq. (10)], and $A_z$ is the area of an antenna/reflecting element at the BS/IRS. The composite $\mathrm{U}_k$-BS channel comprising of the direct and cascaded/reflected channels can be written as

$$\mathbf{v}_k = \mathbf{f}_k + \mathbf{H}\boldsymbol{\Theta}\mathbf{g}_k, \quad (6)$$

where $\boldsymbol{\Theta} = \mathrm{diag}(\varsigma_1 e^{j\theta_1}, \cdots, \varsigma_n e^{j\theta_n}, \cdots, \varsigma_N e^{j\theta_N})$ is the IRS phase-shift matrix. The reflection coefficient of the $n$th IRS element is given by $\varsigma_n e^{j\theta_n}$, where $\varsigma_n \in [0,1]$ and $\theta_n \in [0, 2\pi)$.

### C. Sensing Channel Model

We consider LoS channels to define our sensing channel model which is a typical assumption in the radar literature [8], [12]. The LoS channel between the IRS-BS is already defined in (3). The channels between T-BS and T-IRS can be defined via (4)-(5) as

$$\mathbf{p} = \mathrm{vec}\left(\mathbf{b}_{B1}(\phi_p, \upsilon_p)\mathbf{b}_{B2}^H(\phi_p, \upsilon_p)\right), \quad (7)$$

$$\mathbf{q} = \mathrm{vec}\left(\mathbf{b}_{I1}(\psi_q, \delta_q)\mathbf{b}_{I2}^H(\psi_q, \delta_q)\right), \quad (8)$$

where $\phi_p$ and $\upsilon_p$ are azimuth and elevation of the target with respect to the BS while $\psi_q$ and $\delta_q$ are azimuth and elevation of the target with respect to the IRS.

The composite echo channel can be defined by

$$\mathbf{u} = \alpha_p\mathbf{p} + \alpha_q\bar{\mathbf{H}}\boldsymbol{\Theta}\mathbf{q}, \quad (9)$$

where $\alpha_p$ and $\alpha_q$ are the combined reflection coefficients of the target for the channels $\mathbf{p}$ and $\mathbf{q}$, respectively.

### D. Uplink Channel Estimation

Uplink communication channels are estimated for a given IRS phase-shift matrix ($\boldsymbol{\Theta}$) through the user pilots of length $\tau_p$ denoted by $\boldsymbol{\varrho}_k \in \mathbb{C}^{\tau_p}$. Orthogonal pilots are used to mitigate pilot contamination; $\boldsymbol{\varrho}_k\boldsymbol{\varrho}_{k'}^H = 1$ if $k = k'$, and $\boldsymbol{\varrho}_k\boldsymbol{\varrho}_{k'}^H = 0$ if $k \neq k'$. The pilot signal of the $k$th user received at the BS from the direct and cascaded IRS channels can be written as

$$\mathbf{Y} = \sqrt{\xi}\sum_{k=1}^{K}\mathbf{v}_k\boldsymbol{\varrho}_k + \mathbf{N}, \quad (10)$$

where $\xi = \rho_p\tau_p$ with $\rho_p$ being the average pilot transmit signal-to-noise-ratio (SNR), $\mathbf{v}_k$ is the composite $\mathrm{U}_k$-BS channel in (6), and $\mathbf{N} \sim \mathcal{CN}\left(\mathbf{0}_{M\times\tau_p}, \mathbf{I}_M \otimes \mathbf{I}_{\tau_p}\right)$ is an additive white Gaussian noise (AWGN) matrix. To estimate $\mathbf{v}_k$, we project (10) onto $\boldsymbol{\varrho}_k^H$ as

$$\tilde{\mathbf{y}}_k = \mathbf{Y}\boldsymbol{\varrho}_k^H = \sqrt{\xi}\mathbf{v}_k + \tilde{\mathbf{n}}_k, \quad (11)$$

where $\tilde{\mathbf{n}}_k = \mathbf{N}\boldsymbol{\varrho}_k^H \sim \mathcal{CN}(\mathbf{0}, \mathbf{I}_M)$. By invoking LMMSE estimation upon (11), an estimate for $\mathbf{v}_k$ is derived as [13]

$$\hat{\mathbf{v}}_k = \mathbf{C}_{v_k\tilde{y}_k}\mathbf{C}_{\tilde{y}_k\tilde{y}_k}^{-1}\tilde{\mathbf{y}}_k, \quad (12)$$

where the covariance matrices $\mathbf{C}_{v_k\tilde{y}_k}$ and $\mathbf{C}_{\tilde{y}_k\tilde{y}_k}$ can be derived as (see Appendix A)

$$\mathbf{C}_{v_k\tilde{y}_k} = \sqrt{\xi}\mathbf{C}_{v_k} \quad \text{and} \quad \mathbf{C}_{\tilde{y}_k\tilde{y}_k} = \xi\mathbf{C}_{v_k} + \mathbf{I}, \quad (13)$$

where $\mathbf{C}_{v_k}$ is the covariance matrix of $\mathbf{v}_k$, and it can be derived as (see Appendix A)

$$\mathbf{C}_{v_k} = \mathbf{R}_{f_k} + \bar{\mathbf{H}}\boldsymbol{\Theta}\mathbf{R}_{g_k}\boldsymbol{\Theta}^H\bar{\mathbf{H}}^H + \mathrm{Tr}\left(\mathbf{R}_I\boldsymbol{\Theta}\mathbf{R}_{g_k}\boldsymbol{\Theta}^H\right)\mathbf{R}_T. \quad (14)$$

$$\Xi_{kk} = |\mathrm{Tr}(\mathbf{R}_{f_k}\mathbf{C}_k)|^2 + \mathrm{Tr}\Big(\mathbf{R}_{f_k}\mathbf{C}_k\mathbf{R}_{f_k}\mathbf{C}_k^H\Big) + \mathrm{Tr}\Big(\mathbf{R}_{f_k}\mathbf{C}_k(\mathbf{C}_{v_k}-\mathbf{R}_{f_k})\mathbf{C}_k^H\Big) + \mathrm{Tr}\Big(\mathbf{S}_k\mathbf{C}_k\mathbf{R}_{f_k}\mathbf{C}_k^H\bar{\mathbf{H}}\boldsymbol{\Theta}\Big) + \mathrm{Tr}\Big(\mathbf{Q}_k\mathbf{R}_{f_k}\mathbf{C}_k^H\Big)$$
$$\times \mathrm{Tr}(\mathbf{T}_k) + \big|\mathrm{Tr}\big(\mathbf{S}_k\mathbf{C}_k\bar{\mathbf{H}}\boldsymbol{\Theta}\big)\big|^2 + \mathrm{Tr}\Big(\mathbf{S}_k\mathbf{C}_k\bar{\mathbf{H}}\boldsymbol{\Theta}\mathbf{S}_k\mathbf{C}_k^H\bar{\mathbf{H}}\boldsymbol{\Theta}\Big) + \mathrm{Tr}\Big(\mathbf{S}_k\mathbf{C}_k\tilde{\mathbf{Q}}_k\bar{\mathbf{H}}\boldsymbol{\Theta}\Big)\,\mathrm{Tr}(\mathbf{T}_k) + \mathrm{Tr}\Big(\mathbf{S}_k\mathbf{C}_k\tilde{\mathbf{Q}}_k\bar{\mathbf{H}}\boldsymbol{\Theta}\mathbf{T}_k\Big)$$
$$+ \mathrm{Tr}\Big(\mathbf{S}_k\mathbf{C}_k^H\mathbf{Q}_k\bar{\mathbf{H}}\boldsymbol{\Theta}\Big)\,\mathrm{Tr}(\mathbf{T}_k) + \mathrm{Tr}\Big(\mathbf{S}_k\mathbf{C}_k^H\mathbf{Q}_k\bar{\mathbf{H}}\boldsymbol{\Theta}\mathbf{T}_k\Big) + \big[\mathrm{Tr}(\mathbf{Q}_k)\,\mathrm{Tr}\Big(\tilde{\mathbf{Q}}_k\Big) + \mathrm{Tr}\Big(\mathbf{Q}_k\tilde{\mathbf{Q}}_k\Big)\big]\big[\mathrm{Tr}(\mathbf{T}_k)^2 + \mathrm{Tr}\big((\mathbf{T}_k)^2\big)\big]$$
$$+ \mathrm{Tr}\Big(\tilde{\mathbf{Q}}_k\Big)\big[\mathrm{Tr}\big(\mathbf{S}_k\mathbf{C}_k\bar{\mathbf{H}}\boldsymbol{\Theta}\big)\,\mathrm{Tr}(\mathbf{T}_k) + \mathrm{Tr}\big(\mathbf{S}_k\mathbf{C}_k\bar{\mathbf{H}}\boldsymbol{\Theta}\mathbf{T}_k\big)\big] + \mathrm{Tr}(\mathbf{Q}_k)\big[\mathrm{Tr}\Big(\mathbf{S}_k\mathbf{C}_k^H\bar{\mathbf{H}}\boldsymbol{\Theta}\Big)\,\mathrm{Tr}(\mathbf{T}_k) + \mathrm{Tr}\Big(\mathbf{S}_k\mathbf{C}_k^H\bar{\mathbf{H}}\boldsymbol{\Theta}\mathbf{T}_k\Big)\big]$$
$$+ \mathrm{Tr}(\mathbf{R}_{f_k}\mathbf{C}_k)\big[\mathrm{Tr}\Big(\mathbf{S}_k\mathbf{C}_k^H\bar{\mathbf{H}}\boldsymbol{\Theta}\Big) + \mathrm{Tr}\Big(\tilde{\mathbf{Q}}_k\Big)\,\mathrm{Tr}(\mathbf{T}_k)\big] + \mathrm{Tr}\Big(\mathbf{R}_{f_k}\mathbf{C}_k^H\Big)\big[\mathrm{Tr}\big(\mathbf{S}_k\mathbf{C}_k\bar{\mathbf{H}}\boldsymbol{\Theta}\big) + \mathrm{Tr}(\mathbf{Q}_k)\,\mathrm{Tr}(\mathbf{T}_k)\big]. \quad (25)$$

$$\Xi_{kj} = \mathrm{Tr}\Big(\mathbf{R}_{f_k}\mathbf{C}_j\mathbf{R}_{f_j}\mathbf{C}_j^H\Big) + \mathrm{Tr}\Big(\mathbf{R}_{f_k}\mathbf{C}_j(\mathbf{C}_{v_j}-\mathbf{R}_{f_j})\mathbf{C}_j^H\Big) + \mathrm{Tr}\Big(\mathbf{S}_k\mathbf{C}_j\mathbf{R}_{f_j}\mathbf{C}_j^H\bar{\mathbf{H}}\boldsymbol{\Theta}\Big) + \mathrm{Tr}\Big(\mathbf{Q}_j\mathbf{R}_{f_j}\mathbf{C}_j^H\Big)\,\mathrm{Tr}(\mathbf{T}_k)$$
$$+ \mathrm{Tr}\Big(\mathbf{S}_k\mathbf{C}_j\bar{\mathbf{H}}\boldsymbol{\Theta}\mathbf{S}_j\mathbf{C}_j^H\bar{\mathbf{H}}\boldsymbol{\Theta}\Big) + \mathrm{Tr}\Big(\mathbf{S}_k\mathbf{C}_j\tilde{\mathbf{Q}}_j\bar{\mathbf{H}}\boldsymbol{\Theta}\Big)\,\mathrm{Tr}(\mathbf{T}_j)\,\mathrm{Tr}\Big(\mathbf{S}_j\mathbf{C}_j^H\mathbf{Q}_j\bar{\mathbf{H}}\boldsymbol{\Theta}\Big)\,\mathrm{Tr}(\mathbf{T}_k) + \mathrm{Tr}(\mathbf{Q}_j)\,\mathrm{Tr}\Big(\tilde{\mathbf{Q}}_j\Big)\,\mathrm{Tr}(\mathbf{T}_k\mathbf{T}_j)$$
$$+ \mathrm{Tr}\Big(\mathbf{Q}_j\tilde{\mathbf{Q}}_j\Big)\,\mathrm{Tr}(\mathbf{T}_k)\,\mathrm{Tr}(\mathbf{T}_j) + \mathrm{Tr}\Big(\tilde{\mathbf{Q}}_j\Big)\,\mathrm{Tr}\big(\mathbf{S}_k\mathbf{C}_j\bar{\mathbf{H}}\boldsymbol{\Theta}\mathbf{T}_j\big)\,\mathrm{Tr}(\mathbf{Q}_j)\,\mathrm{Tr}\Big(\mathbf{S}_j\mathbf{C}_j^H\bar{\mathbf{H}}\boldsymbol{\Theta}\mathbf{T}_k\Big). \quad (26)$$

Due to orthogonality criterion of LMMSE estimation [13], $\mathbf{v}_k$ can be written in terms of its estimate ($\hat{\mathbf{v}}_k$) and estimation error ($\boldsymbol{\epsilon}_k$) as $\mathbf{v}_k = \hat{\mathbf{v}}_k + \boldsymbol{\epsilon}_k$, where $\boldsymbol{\epsilon}_{v_k}$ is a zero mean Gaussian vector having a covariance matrix $\mathbf{C}_{\epsilon_{v_k}} = \mathbf{C}_{v_k} - \mathbf{C}_{\hat{v}_k}$. The error is uncorrelated with its estimator $\hat{\mathbf{v}}_k$ [13]. The covariance matrix ($\mathbf{C}_{\hat{v}_k}$) of $\hat{\mathbf{v}}_k$ in (12) can be derived as (Appendix A)

$$\mathbf{C}_{\hat{v}_k} = \mathbf{C}_{v_k\tilde{y}_k}\mathbf{C}_{\tilde{y}_k\tilde{y}_k}^{-1}\mathbf{C}_{v_k\tilde{y}_k}. \quad (15)$$

### *E. Communication Signal Model*

The downlink (DL) data precoder for $\mathrm{U}_k$ is constructed by applying MRT principle to the composite channel $\mathbf{v}_k$ due to its simplicity for massive MIMO [8]. The sensing precoder is designed to maximize the received power of the echo signal at the BS receive array by using MRT principle to the composite echo signal. The joint ISAC precoder is then given by

$$\mathbf{w}_k = \sqrt{\eta_{k,c}}\hat{\mathbf{v}}_k + \sqrt{\eta_{k,s}}\mathbf{u}, \quad (16)$$

where $\hat{\mathbf{v}}_k$ is the LMMSE estimate of $\mathbf{v}_k$ for the $k$th user, and $\mathbf{u}$ is the composite echo channel in (9). In (16), the power normalization/allocation factors for the precoders are defined as $\eta_{k,c} = \tilde{\eta}_{k,c}/\mathrm{Tr}(\mathbf{C}_{\hat{v}_k})$ and $\eta_{k,s} = \tilde{\eta}_{k,s}/\mathrm{Tr}\big(\mathbf{u}\mathbf{u}^H\big)$ in which $\tilde{\eta}_{k,c}$ and $\tilde{\eta}_{k,s}$ are the power allocation coefficients for the communication and sensing signals.

The received signal at $\mathrm{U}_k$ can be written as

$$y_k = \sqrt{\rho}\mathbf{v}_k^H\mathbf{w}_k x_k + \sqrt{\rho}\sum\nolimits_{j\neq k}^{K}\mathbf{v}_k^H\mathbf{w}_j x_j + n_k, \quad (17a)$$
$$= \sqrt{\rho}\mathbb{E}\Big[\mathbf{v}_k^H\mathbf{w}_k x_k\Big] + \sqrt{\rho}(\mathbf{v}_k^H\mathbf{w}_k x_k - \mathbb{E}\Big[\mathbf{v}_k^H\mathbf{w}_k x_k\Big]) + \sum\nolimits_{j\neq k}^{K}\sqrt{\rho}\mathbf{v}_k^H\mathbf{w}_j x_j + n_k, \quad (17b)$$

where $\rho$ is the transmit SNR at the BS, $x_k$ is the data symbol intended for $\mathrm{U}_k$, satisfying $\mathbb{E}\big[|x_k|^2\big] = 1$, and $n_k \sim \mathcal{CN}(0,1)$ is the AWGN at $\mathrm{U}_k$. The first term in (17b) is the desired signal, the second term represents decision uncertainty, and the third term denotes inter-user-interference. The second equality (17b) is written to emphasize the fact that users rely on statistical CSI to decode DL data.

### *F. Sensing Signal Model*

The BS signal is reflected back, and this echo is received by the BS receive array as

$$\bar{\mathbf{y}} = \sqrt{\rho}\mathbf{u}\mathbf{u}^H\mathbf{W}\mathbf{x} + \bar{\mathbf{n}}, \quad (18)$$

where $\mathbf{W} = [\mathbf{w}_1, ..., \mathbf{w}_k, ..., \mathbf{w}_K] \in \mathbb{C}^{M\times K}$, $\mathbf{x} = [x_1, ..., x_k, ..., x_K]^T \in \mathbb{C}^K$, and $\bar{\mathbf{n}} \in \mathbb{C}^M$ is an AWGN with i.i.d. entries from $\mathcal{CN}(0,1)$. The sensing combiner is designed as $\mathbf{u}^H$ to maximize the received echo power as

$$\bar{y} = \underbrace{\sqrt{\rho}\mathbf{u}^H\mathbf{u}\mathbf{u}^H\mathbf{W}\mathbf{x}}_{DE} + \bar{n}, \quad (19)$$

where $\bar{n} = \mathbf{u}^H\bar{\mathbf{n}}$, and the first term in (19) is the desired echo.

## III. Performance analysis

### *A. An achievable rate for the communication users*

By invoking the worst-case Gaussian technique [8] to (17a), an achievable user rate can be defined as

$$\mathcal{R}_k = \kappa\log_2(1+\gamma_k), \quad (20)$$

where $\kappa = (\tau_c - \tau_p)/\tau_c$ with $\tau_c$ being the channel coherence interval, and $\gamma_k$ is the SINR at $\mathrm{U}_k$, which can be derived as (see Appendix B)

$$\gamma_k = \frac{|DS_k|^2}{DU_k + \sum_{j\neq k}^{K} IUI_{kj} + 1}, \quad (21)$$

where $DS_k$, $DU_k$, and $IUI_{kj}$ can be derived as

$$DS_k = \sqrt{\rho}\mathbb{E}\Big[\mathbf{v}_k^H\mathbf{w}_k x_k\Big] = \sqrt{\eta_{k,c}\rho}\mathrm{Tr}(\mathbf{C}_{\hat{v}_k}), \quad (22)$$
$$DU_k = \rho\mathbb{V}\mathrm{ar}\Big[\mathbf{v}_k^H\mathbf{w}_k x_k\Big] = \eta_{k,c}\rho\xi\Xi_{kk} + \eta_{k,c}\rho\mathrm{Tr}\Big(\mathbf{C}_{v_k}\mathbf{C}_k\mathbf{C}_k^H\Big) + \eta_{k,s}\rho\mathrm{Tr}\Big(\mathbf{C}_{v_k}\mathbf{u}\mathbf{u}^H\Big) - |DS_k|^2, \quad (23)$$
$$IUI_{kj} = \rho\mathbb{E}\Big[|\mathbf{v}_k^H\mathbf{w}_j x_j|^2\Big] = \eta_{j,c}\rho\xi\Xi_{kj} + \eta_{j,c}\rho\mathrm{Tr}\Big(\mathbf{C}_{v_k}\mathbf{C}_j\mathbf{C}_j^H\Big) + \eta_{j,s}\rho\mathrm{Tr}\Big(\mathbf{C}_{v_k}\mathbf{u}\mathbf{u}^H\Big), \quad (24)$$

where $\Xi_{kk}$ and $\Xi_{kj}$ can be derived as (25) and (26), respectively, as shown at the top of this page. In (25)-(26), we denote $\mathbf{C}_k = \mathbf{C}_{v_k\tilde{y}_k}\mathbf{C}_{\tilde{y}_k\tilde{y}_k}^{-1}$, $\mathbf{T}_k = \mathbf{R}_{g_k}\boldsymbol{\Theta}^H\mathbf{R}_I\boldsymbol{\Theta}$, $\mathbf{Q}_k = \mathbf{R}_T\mathbf{C}_k$, $\tilde{\mathbf{Q}}_k = \mathbf{R}_T\mathbf{C}_k^H$, and $\mathbf{S}_k = \mathbf{R}_{g_k}\boldsymbol{\Theta}^H\bar{\mathbf{H}}^H$.

### *B. A signal-to-noise-ratio for sensing*

An average sensing SNR at the BS is given by

$$\gamma_s = \mathbb{E}\big[|DE|^2/|\bar{n}|^2\big], \quad (27)$$

To evaluate $\gamma_s$ in (25), we resort to a tight approximation as [10, Lemma 1]

$$\gamma \approx \mathbb{E}\big[|DE|^2\big]/\mathbb{E}\big[|\bar{n}|^2\big], \quad (28)$$

where $\mathbb{E}\big[|DE|^2\big]$ and $\mathbb{E}\big[|\bar{n}|^2\big]$ are derived as (Appendix C)

$$\mathbb{E}\big[|DE|^2\big] = \rho\mathrm{Tr}\Big(\mathbf{u}\mathbf{u}^H\Big)^2\sum_{k=1}^{K}\eta_{k,c}\mathbf{u}^H\mathbf{C}_{\hat{v}_k}\mathbf{u} + \eta_{k,s}\mathrm{Tr}\Big(\mathbf{u}\mathbf{u}^H\Big)^2, \quad (29)$$
$$\sigma_s^2 = \mathbb{E}\big[|\bar{n}|^2\big] = \mathrm{Tr}\Big(\mathbf{u}\mathbf{u}^H\Big). \quad (30)$$

## IV. IRS Phase-Shift Optimization

By adopting statistical CSI, the IRS phase-shift matrix $\boldsymbol{\Theta}$ can be optimized to maximize the minimum average power of the composite communication channel for the $k$th user ($\mathrm{U}_k$), while satisfying an average power threshold for the reflected sensing channel. This optimization problem is formulated as

$$\mathcal{P}: \max_{\boldsymbol{\Theta}} \min_{k} \quad \mathrm{Tr}(\mathbf{C}_{v_k}), \tag{31a}$$

$$\text{subject to} \quad \mathrm{C}_1: \mathrm{Tr}\Big(\mathbf{u}\mathbf{u}^H\Big) \geq \mu, \tag{31b}$$

$$\mathrm{C}_2: \Big|[\boldsymbol{\Theta}]_{n,n}\Big|^2 = 1 \ \forall n. \tag{31c}$$

where $\mu$ is a predefined threshold for the average sensing channel power. We assume that $\varsigma_n = 1$ for $n \in \{1, \cdots, N\}$, which is a common assumption in IRS literature [9]. By defining a common lower bound $\delta$ for the objective function in (31a), the original optimization problem (31a)-(31c) can be reformulated equivalently as

$$\mathcal{P}: \max_{\boldsymbol{\Theta}} \quad \delta, \tag{32a}$$

$$\text{subject to} \quad \mathrm{C}_1: \mathrm{Tr}\Big(\mathbf{u}\mathbf{u}^H\Big) \geq \mu, \tag{32b}$$

$$\mathrm{C}_2: \mathrm{Tr}(\mathbf{C}_{v_k}) \geq \delta \ \forall k. \tag{32c}$$

$$\mathrm{C}_3: \Big|[\boldsymbol{\Theta}]_{n,n}\Big|^2 = 1 \ \forall n, \tag{32d}$$

From (14), by using the fact that $\mathbf{u} = \alpha_p \mathbf{p} + \alpha_q \bar{\mathbf{H}} \boldsymbol{\Theta} \mathbf{q}$ and $\mathbf{R}_{g_k} = \zeta_{g_k} \mathbf{R}_I$, the constraints $\mathrm{C}_1$ in (32b) and $\mathrm{C}_2$ in (32c) can be rewritten as

$$\mathrm{C}_1: \alpha_p^2 \mathrm{Tr}\Big(\mathbf{p}\mathbf{p}^H\Big) + 2\alpha_p\alpha_q \mathrm{Re}\left(\mathrm{Tr}\Big(\bar{\mathbf{H}}^H \mathbf{p}\mathbf{q}^H \boldsymbol{\Theta}^H\Big)\right) + \alpha_q^2 \mathrm{Tr}\Big(\bar{\mathbf{H}}^H \bar{\mathbf{H}} \boldsymbol{\Theta} \mathbf{q}\mathbf{q}^H \boldsymbol{\Theta}^H\Big) \geq \mu, \tag{33}$$

$$\mathrm{C}_2: \mathrm{Tr}(\mathbf{R}_{f_k}) + \zeta_{g_k} \mathrm{Tr}\Big(\bar{\mathbf{H}}^H \bar{\mathbf{H}} \boldsymbol{\Theta} \mathbf{R}_I \boldsymbol{\Theta}^H\Big) + \zeta_{g_k} \mathrm{Tr}\Big(\mathbf{R}_I \boldsymbol{\Theta} \mathbf{R}_I \boldsymbol{\Theta}^H\Big) \mathrm{Tr}(\mathbf{R}_T) \geq \delta \ \forall k. \tag{34}$$

By denoting $\tilde{\boldsymbol{\theta}} = \left[\mathrm{e}^{j\theta_1}, ..., \mathrm{e}^{j\theta_N}\right] \in \mathbb{C}^{1\times N}$, $\tilde{\mathbf{d}} = \mathrm{diag}(\bar{\mathbf{H}}^H \mathbf{p}\mathbf{q}^H)^T \in \mathbb{C}^{1\times N}$, $\tilde{\mathbf{R}}_{Hq} = (\bar{\mathbf{H}}^H \bar{\mathbf{H}})^T \odot (\mathbf{q}\mathbf{q}^H) \in \mathbb{C}^{N\times N}$, $\tilde{\mathbf{R}}_{II} = \mathbf{R}_I \odot \mathbf{R}_I \in \mathbb{C}^{N\times N}$, and $\tilde{\mathbf{R}}_{HI} = (\bar{\mathbf{H}}^H \bar{\mathbf{H}})^T \odot \mathbf{R}_I \in \mathbb{C}^{N\times N}$, the traces in (33) and (34) can be written as [14]

$$\mathrm{Tr}\Big(\bar{\mathbf{H}}^H \mathbf{p}\mathbf{q}^H \boldsymbol{\Theta}^H\Big) = \tilde{\mathbf{d}} \tilde{\boldsymbol{\theta}}^H, \ \mathrm{Tr}\Big(\bar{\mathbf{H}}^H \bar{\mathbf{H}} \boldsymbol{\Theta} \mathbf{q}\mathbf{q}^H \boldsymbol{\Theta}^H\Big) = \tilde{\boldsymbol{\theta}} \tilde{\mathbf{R}}_{Hq} \tilde{\boldsymbol{\theta}}^H, \tag{35}$$

$$\mathrm{Tr}\Big(\mathbf{R}_I \boldsymbol{\Theta} \mathbf{R}_I \boldsymbol{\Theta}^H\Big) = \tilde{\boldsymbol{\theta}} \tilde{\mathbf{R}}_{II} \tilde{\boldsymbol{\theta}}^H, \ \mathrm{Tr}\Big(\bar{\mathbf{H}}^H \bar{\mathbf{H}} \boldsymbol{\Theta} \mathbf{R}_I \boldsymbol{\Theta}^H\Big) = \tilde{\boldsymbol{\theta}} \tilde{\mathbf{R}}_{HI} \tilde{\boldsymbol{\theta}}^H. \tag{36}$$

Thereby, (33) and (34) can be written as

$$\mathrm{C}_1: \alpha_p^2 \mathrm{Tr}\Big(\mathbf{p}\mathbf{p}^H\Big) + 2\alpha_p\alpha_q \mathrm{Re}(\tilde{\mathbf{d}} \tilde{\boldsymbol{\theta}}^H) + \alpha_q^2 \tilde{\boldsymbol{\theta}} \tilde{\mathbf{R}}_{Hq} \tilde{\boldsymbol{\theta}}^H \geq \mu, \tag{37}$$

$$\mathrm{C}_2: \mathrm{Tr}(\mathbf{R}_{f_k}) + \zeta_{g_k} \tilde{\boldsymbol{\theta}} \tilde{\mathbf{R}} \tilde{\boldsymbol{\theta}}^H \geq \delta \ \forall k, \tag{38}$$

where $\tilde{\mathbf{R}} = \tilde{\mathbf{R}}_{HI} + \tilde{\mathbf{R}}_{II} \mathrm{Tr}(\mathbf{R}_T)$. The optimization problem in (32a)-(32d) can be reformulated by using (37) and (38) as

$$\mathcal{P}: \max_{\boldsymbol{\Theta}} \quad \delta, \tag{39a}$$

$$\text{subject to} \quad \mathrm{C}_1: \bar{\boldsymbol{\theta}} \bar{\mathbf{R}} \bar{\boldsymbol{\theta}}^H \geq \mu, \tag{39b}$$

$$\mathrm{C}_2: \bar{\boldsymbol{\theta}} \bar{\mathbf{R}}_k \bar{\boldsymbol{\theta}}^H \geq \delta \ \forall k, \tag{39c}$$

$$\mathrm{C}_3: \big|[\bar{\boldsymbol{\theta}}]_n\big|^2 = 1 \ \forall n, \tag{39d}$$

where $\bar{\boldsymbol{\theta}}$ is $[\tilde{\boldsymbol{\theta}}_{1\times N} \ 1]$, and $\bar{\mathbf{R}}$ and $\bar{\mathbf{R}}_k$ are defined as

$$\bar{\mathbf{R}} = \begin{bmatrix} \left[\alpha_q^2 \tilde{\mathbf{R}}_{Hq}\right]_{N\times N} & \left[\alpha_p\alpha_q \tilde{\mathbf{d}}^H\right]_{N\times 1} \\ \left[\alpha_p\alpha_q \tilde{\mathbf{d}}\right]_{1\times N} & \alpha_p^2 \mathrm{Tr}\big(\mathbf{p}\mathbf{p}^H\big) \end{bmatrix}, \tag{40}$$

$$\bar{\mathbf{R}}_k = \begin{bmatrix} \left[\zeta_{g_k} \tilde{\mathbf{R}}_C\right]_{N\times N} & [\mathbf{0}]_{N\times 1} \\ [\mathbf{0}]_{1\times N} & \mathrm{Tr}(\mathbf{R}_{f_k}) \end{bmatrix}. \tag{41}$$

The constraints $\mathrm{C}_1$ in (39b) and $\mathrm{C}_2$ in (39c) are still non-convex. By denoting the value of $\bar{\boldsymbol{\theta}}$ during $t$th iteration as $\bar{\boldsymbol{\theta}}_t$, $\mathrm{C}_1$ and $\mathrm{C}_2$ can be approximated via lower bounds as [14]

$$\bar{\boldsymbol{\theta}} \bar{\mathbf{R}} \bar{\boldsymbol{\theta}}^H \geq \bar{\boldsymbol{\theta}}_t \bar{\mathbf{R}} \bar{\boldsymbol{\theta}}_t^H + 2\mathrm{Re}\left((\bar{\boldsymbol{\theta}} - \bar{\boldsymbol{\theta}}_t) \bar{\mathbf{R}} \bar{\boldsymbol{\theta}}_t^H\right) = \Gamma(\bar{\boldsymbol{\theta}}), \tag{42}$$

$$\bar{\boldsymbol{\theta}} \bar{\mathbf{R}}_k \bar{\boldsymbol{\theta}}^H \geq \bar{\boldsymbol{\theta}}_t \bar{\mathbf{R}}_k \bar{\boldsymbol{\theta}}_t^H + 2\mathrm{Re}\left((\bar{\boldsymbol{\theta}} - \bar{\boldsymbol{\theta}}_t) \bar{\mathbf{R}}_k \bar{\boldsymbol{\theta}}_t^H\right) = \Psi_k(\bar{\boldsymbol{\theta}}) \ \forall k. \tag{43}$$

In (42), and (43), the equality holds when $\bar{\boldsymbol{\theta}} = \bar{\boldsymbol{\theta}}_t$. Moreover, the strict modulus constraint of $\mathrm{C}_2$ in (39d) is relaxed as

$$\mathrm{C}_2': \big|[\bar{\boldsymbol{\theta}}]_n\big|^2 \leq 1, \ \forall n. \tag{44}$$

The optimization problem in (39a)-(39d) during the $t$th iteration is reformulated via (42)-(44) to be a convex form as

$$\mathcal{P}_t: \max_{\bar{\boldsymbol{\theta}}} \quad \delta, \tag{45a}$$

$$\text{subject to} \quad \mathrm{C}_1': \Gamma(\bar{\boldsymbol{\theta}}) \geq \mu, \tag{45b}$$

$$\mathrm{C}_2': \big|[\bar{\boldsymbol{\theta}}]_n\big|^2 \leq 1 \ \forall n, \tag{45c}$$

$$\mathrm{C}_3': \Psi_k(\bar{\boldsymbol{\theta}}) \geq \delta \ \forall k, \tag{45d}$$

$$\mathrm{C}_4: [\bar{\boldsymbol{\theta}}]_{N+1} = 1. \tag{45e}$$

Since $\mathcal{P}_t$ in (45a)-(45e) can be cast as a quadratically constrained quadratic optimization problem, it can be solved via CVX or Gurobi [15]. To satisfy the strict modulus constraint in (45e), we divide each element of the optimized $\bar{\boldsymbol{\theta}}$ vector obtained by solving $\mathcal{P}_t$ by its magnitude in each iteration [14]

$$[\bar{\boldsymbol{\theta}}_t^*]_n = [\bar{\boldsymbol{\theta}}_t']_n \Big/ \big|[\bar{\boldsymbol{\theta}}_t']_n\big|, \quad \forall n = \{1 \cdots N\}, \tag{46}$$

where $\bar{\boldsymbol{\theta}}_t^*$ and $\bar{\boldsymbol{\theta}}_t'$ are the solutions of the $t$th iteration of $\mathcal{P}$ and $\mathcal{P}_t$. This optimization procedure is summarized in Algorithm 1. Its complexity scales as $\mathcal{O}(N^{3.5})$ [16], and the overall complexity raises to $\mathcal{O}(TN^{3.5})$ with $T$ iterations.

**Algorithm 1** : An algorithm to solve $\mathcal{P}$ in (31a)-(31c)

**Input:** $\zeta_{g_k}, \alpha_p, \alpha_q, \mu, \mathbf{p}, \mathbf{q}, \mathbf{R}_I, \mathbf{R}_T, \mathbf{R}_{f_k}, \bar{\mathbf{H}} \ \forall k$
**Output:** $\boldsymbol{\Theta}^*$
**Initialization:** Set $\boldsymbol{\Theta}_0$, $\bar{\boldsymbol{\theta}}_0 = \mathrm{diag}(\boldsymbol{\Theta}_0)^T$, $t = 0$
1: Compute $\tilde{\mathbf{d}} = \mathrm{diag}(\bar{\mathbf{H}}^H \mathbf{p}\mathbf{q}^H)^T$, $\tilde{\mathbf{R}}_{Hq} = (\bar{\mathbf{H}}^H \bar{\mathbf{H}})^T \odot \mathbf{q}\mathbf{q}^H$, $\tilde{\mathbf{R}}_{II} = \mathbf{R}_I \odot \mathbf{R}_I$, $\tilde{\mathbf{R}}_{HI} = (\bar{\mathbf{H}}^H \bar{\mathbf{H}})^T \odot \mathbf{R}_I$
2: Compute $\bar{\mathbf{R}}$ and $\bar{\mathbf{R}}_k \ \forall k$
**Repeat:**
3: Compute $\bar{\boldsymbol{\theta}}_t'$ by solving $\mathcal{P}_t$ in (45a)-(45d)
4: Update $\bar{\boldsymbol{\theta}}_t^*$(46) and set $[\boldsymbol{\Theta}_t]_{n,n} = [\bar{\boldsymbol{\theta}}_t^*]_n$, $\forall n = \{1 \cdots N\}$
5: $t = t + 1$,
**Until** Convergence

## V. Sensing performance evaluation

We invoke 2D MUSIC algorithm [17] to estimate the target location through the elevation and azimuth angles, while keeping the angles between BS and IRS fixed. We suppose that $\bar{\tau} = \tau_c - \tau_p$ snapshots are available at the BS for target detection. The sample covariance matrix for the MUSIC algorithm can be written via (18) as

$$\mathbf{R}_s = \frac{1}{\bar{\tau}} \sum\nolimits_{n=1}^{\bar{\tau}} \bar{\mathbf{y}}[n] (\bar{\mathbf{y}}[n])^H. \tag{47}$$

where $\bar{\mathbf{y}}[n]$ represents the $n$th snapshot of the received signal. The noise subspace $\mathbf{Z} \in \mathbb{C}^{M_R \times (M_R - 1)}$ for the target can be constructed by computing the eigenvectors of $\mathbf{R}_s$ corresponding to $M_R - 1$ number of lowest eigenvalues. We define $\mathbf{u}$ in (9) as $\mathbf{u} = \mathbf{u}(\phi_p, \upsilon_p, \psi_q, \delta_q)$ as it is a function of the target angles with respect to the BS ($\phi_p$ and $\upsilon_p$) and the IRS ($\psi_q$ and $\delta_q$). Then, the spatial spectrum can be written as [17]

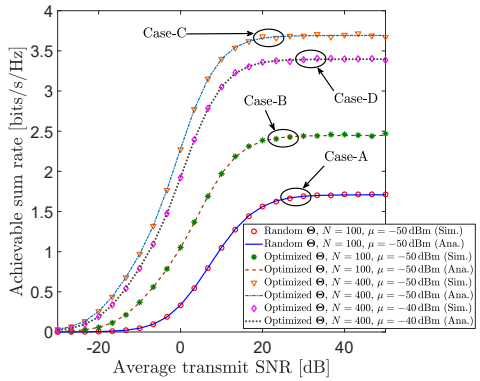


Fig. 2. The achievable rate versus the average transmit SNR ($\rho$) .

$$\mathbf{S}(\mathbf{r}_i) = [\mathbf{u}^H(\phi_{pi}, \upsilon_{pi}, \psi_{qi}, \delta_{qi})\mathbf{Z}\mathbf{Z}^H\mathbf{u}(\phi_{pi}, \upsilon_{pi}, \psi_{qi}, \delta_{qi})]^{-1}, \quad (48)$$

where $\phi_{pi}$/$\psi_{qi}$, and $\upsilon_{pi}$/$\delta_{qi}$ are azimuth and elevation angles of target from BS/IRS, respectively at the $i$th point in the 3D grid. Then, the target location can be estimated by locating the peaks of $\mathbf{S}(\mathbf{r}_i)$ by adopting a grid searching method [17].

## VI. Numerical Results

We set $M = 400$, $N = 100$, and $K = 5$. The distances of IRS-BS, $\mathrm{U}_k$-BS, $\mathrm{U}_k$-IRS, T-BS, and T-IRS are randomly generated from the range $[50,\ 200]$ m, and Rician factor is set to $K \in [1.0, 3.0]$. The path-loss for communication channels is modeled by using the 3GPP Urban Micro-cell model [18, Table 5.1], while setting the carrier frequency to 3 GHz. The target reflection coefficient is modeled as $\alpha_z^2 = \sqrt{\beta_z}\vartheta_z$, where $\beta_z$ is the sensing channel gain, and $\vartheta_z \sim \mathcal{CN}(0,1)$ is the radar cross section (RCS) for $z \in \{p, q\}$ [12]. Here, $\beta_z = \lambda^2\sigma_z^2/((4\pi)^3 d_z^4)$, where $\lambda$, $\sigma_z^2$, and $d_z$ are the wavelength, RCS variance, distance of the channel $z$, respectively [12]. The coherence interval $\tau_c = 196$ [8], and the pilot length is set to $\tau_P = K$. The UL pilot transmit SNR is set to 0 dB.

In Fig. 2, an achievable sum rate comparison is presented for four different cases/set-ups. The random IRS phase-shifts are used in Case-A as a baseline, and the phase-shifts are optimized based on Algorithm-1 in Case-B, -C, and -D. By comparing Case-A with Case-B, we observe that a sum rate gain of $52.08\%$ can be obtained at an average transmit SNR of $\rho = 20$ dB by using our optimized phase-shifts over the random counterparts. From Case-B and Case-C, we also reveal that by increasing $N = 100$ to $N = 400$, about $53.91\%$ sum rate gain can be achieved at $\rho = 20$ dB. Fig. 2 further shows that the sum rate increases when the number of passive reflective IRS elements ($N$) increases. For instance, at $\rho = 20$ dB with $N = 400$ and optimized IRS phase-shits, Case-C with $\mu = -50$ dBm outperforms Case-D with $\mu = -40$ dBm by about $9.04\%$ in terms of the sum rate. We further reveal that the sum rate decreases when increasing the predefined average sensing channel power threshold in Algorithm-1. This clearly unveils the sensing-communication trade-off of ISAC.

In Fig. 3 and Fig. 4, the 2D MUSIC algorithm is used to locate the target with respect the BS and IRS. Hence, the peaks of the MUSIC spectrum correspond to the target. From Fig. 2, we observe that the azimuth and elevation angles of AoAs for the target with respect to the BS are $(\theta_p, \upsilon_p) = (20°, -40°)$.

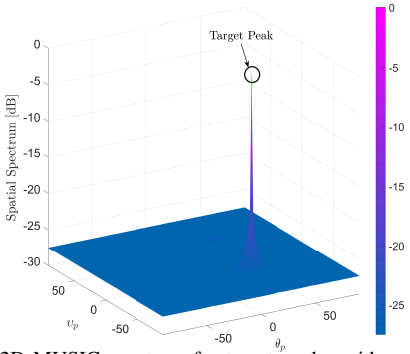


Fig. 3. The 2D MUSIC spectrum for target angles with respect to the BS.

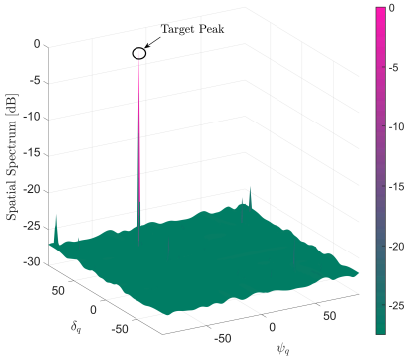


Fig. 4. The 2D MUSIC spectrum for target angles with respect to the IRS.

From Fig. 4, we determine the target AoAs with respect to the IRS as $(\psi_q, \delta_q) = (-30°, 50°)$. All these estimated angles through the 2D MUSIC algorithm accurately match with the AoAs that we have set in the simulation setup. Hence, Fig. 2 and Fig. 3 show that the MUSIC algorithm can be used to locate the target with respect to both the BS and IRS in an massive MIMO ISAC even with linear MRT-based precoders.

## VII. Conclusion

The performance of an IRS-aided massive MIMO ISAC system has been investigated. The uplink channels have been estimated via the LMMSE techniques, and the estimated CSI is used to construct the user precoders. The IRS phase-shifts have been optimized based on statistical CSI to maximize the average power gain of the composite channel of the weakest communication user while satisfying a predefined average power threshold for sensing channel. An achievable user rate has been derived in closed-form, and it captures spatially correlated Rician fading and imperfect CSI. The peaks of the 2D MUSIC spectrum function have been determined via a grid-search to locate the target. Our numerical results demonstrate the potential of IRS-aided massive MIMO ISAC systems in improving the performance trade-offs between sensing and communication tasks.

## Appendix A
## Derivation of $\mathbf{C}_{v_k}$, $\mathbf{C}_{v_k\tilde{y}_k}$, $\mathbf{C}_{\tilde{y}_k\tilde{y}_k}$, and $\mathbf{C}_{\hat{v}_k}$

The covariance matrix of the true composite channel ($\mathbf{v}_k$) of the $k$th user in (6) can be derived as

$$\begin{aligned}\mathbf{C}_{v_k} &= \mathbb{E}\left[(\mathbf{v}_k - \mathbb{E}[\mathbf{v}_k])(\mathbf{v}_k - \mathbb{E}[\mathbf{v}_k])^H\right] \\ &= \mathbb{E}\left[(\mathbf{f}_k + \mathbf{H}\boldsymbol{\Theta}\mathbf{g}_k)(\mathbf{f}_k + \mathbf{H}\boldsymbol{\Theta}\mathbf{g}_k)^H\right]\end{aligned}$$

$$\mathbb{E}\left[\left|\mathbf{v}_k^H\mathbf{C}_k\mathbf{v}_k\right|^2\right]=\mathbb{E}\left[\left|\mathbf{f}_k^H\mathbf{C}_k\mathbf{f}_k\right|^2\right]+\mathbb{E}\left[\left|\mathbf{f}_k^H\mathbf{C}_k\mathbf{H}\boldsymbol{\Theta}\mathbf{g}_k\right|^2\right]+\mathbb{E}\left[\left|\mathbf{g}_k^H\boldsymbol{\Theta}^H\mathbf{H}^H\mathbf{C}_k\mathbf{f}_k\right|^2\right]+\mathbb{E}\left[\left|\mathbf{g}_k^H\boldsymbol{\Theta}^H\mathbf{H}^H\mathbf{C}_k\mathbf{H}\boldsymbol{\Theta}\mathbf{g}_k\right|^2\right]$$
$$+\mathbb{E}\left[\mathbf{f}_k^H\mathbf{C}_k\mathbf{f}_k\mathbf{g}_k^H\boldsymbol{\Theta}^H\mathbf{H}^H\mathbf{C}_k^H\mathbf{H}\boldsymbol{\Theta}\mathbf{g}_k\right]+\mathbb{E}\left[\mathbf{g}_k^H\boldsymbol{\Theta}^H\mathbf{H}^H\mathbf{C}_k\mathbf{H}\boldsymbol{\Theta}\mathbf{g}_k\mathbf{f}_k^H\mathbf{C}_k^H\mathbf{f}_k\right]. \quad (55)$$

$$\mathbb{E}\left[\left|\mathbf{v}_k^H\mathbf{C}_j\mathbf{v}_j\right|^2\right]=\mathbb{E}\left[\left|\mathbf{f}_k^H\mathbf{C}_j\mathbf{f}_j\right|^2\right]+\mathbb{E}\left[\left|\mathbf{f}_k^H\mathbf{C}_j\mathbf{H}\boldsymbol{\Theta}\mathbf{g}_j\right|^2\right]+\mathbb{E}\left[\left|\mathbf{g}_k^H\boldsymbol{\Theta}^H\mathbf{H}^H\mathbf{C}_j\mathbf{f}_j\right|^2\right]+\mathbb{E}\left[\left|\mathbf{g}_k^H\boldsymbol{\Theta}^H\mathbf{H}^H\mathbf{C}_j\mathbf{H}\boldsymbol{\Theta}\mathbf{g}_j\right|^2\right]. \quad (57)$$

$$=\mathbf{R}_{f_k}+\bar{\mathbf{H}}\boldsymbol{\Theta}\mathbf{R}_{g_k}\boldsymbol{\Theta}^H\bar{\mathbf{H}}^H+\mathbf{R}_T\mathbb{E}[\tilde{\mathbf{H}}\mathbf{R}_I^{\frac{1}{2}}\boldsymbol{\Theta}\mathbf{R}_{g_k}\boldsymbol{\Theta}^H\mathbf{R}_I^{\frac{1}{2}H}\tilde{\mathbf{H}}^H]$$
$$\overset{(a)}{=}\mathbf{R}_{f_k}+\bar{\mathbf{H}}\boldsymbol{\Theta}\mathbf{R}_{g_k}\boldsymbol{\Theta}^H\bar{\mathbf{H}}^H+\mathrm{Tr}(\mathbf{R}_I\boldsymbol{\Theta}\mathbf{R}_{g_k}\boldsymbol{\Theta}^H)\mathbf{R}_T, \quad (49)$$

where the step $(a)$ is derived via [19, Lemma 8]. Then, $\mathbf{C}_{v_k\tilde{y}_k}$ and $\mathbf{C}_{\tilde{y}_k\tilde{y}_k}$ in (13) can be derived as

$$\mathbf{C}_{v_k\tilde{y}_k}=\mathbb{E}\left[(\mathbf{v}_k-\mathbb{E}[\mathbf{v}_k])(\tilde{\mathbf{y}}_k-\mathbb{E}[\tilde{\mathbf{y}}_k])^H\right]$$
$$=\mathbb{E}\left[\mathbf{v}_k(\sqrt{\xi}\mathbf{v}_k+\tilde{\mathbf{n}}_k)^H\right]=\sqrt{\xi}\mathbf{C}_{v_k}, \quad (50)$$
$$\mathbf{C}_{\tilde{y}_k\tilde{y}_k}=\mathbb{E}\left[(\tilde{\mathbf{y}}_k-\mathbb{E}[\tilde{\mathbf{y}}_k])(\tilde{\mathbf{y}}_k-\mathbb{E}[\tilde{\mathbf{y}}_k])^H\right]$$
$$=\mathbb{E}\left[(\sqrt{\xi}\mathbf{v}_k+\tilde{\mathbf{n}}_k)(\sqrt{\xi}\mathbf{v}_k+\tilde{\mathbf{n}}_k)^H\right]=\xi\mathbf{C}_{v_k}+\mathbf{I}_M. \quad (51)$$

The covariance matrix of the LMMSE estimate ($\hat{\mathbf{v}}_k$) of the composite channel of the $k$th user ($\mathbf{v}_k$) can be derived as

$$\mathbf{C}_{\hat{v}_k}=\mathbb{E}[\hat{\mathbf{v}}_k\hat{\mathbf{v}}_k]=\mathbb{E}\left[(\mathbf{C}_{v_k\tilde{y}_k}\mathbf{C}_{\tilde{y}_k\tilde{y}_k}^{-1}\tilde{\mathbf{y}})(\mathbf{C}_{v_{al}\tilde{y}}\mathbf{C}_{\tilde{y}_{al}\tilde{y}_{al}}^{-1}\tilde{\mathbf{y}_{al}})^H\right]$$
$$=\mathbf{C}_{v_k\tilde{y}_k}\mathbf{C}_{\tilde{y}_k\tilde{y}_k}^{-1}\mathbf{C}_{v_k\tilde{y}_k}. \quad (52)$$

## Appendix B
## Derivation of $\mathcal{R}_k$ in (20)

The term $DS_k$ in (22) can be derived as

$$DS_k=\sqrt{\rho}\mathbb{E}\left[\mathbf{v}_k^H\mathbf{w}_kx_k\right]=\sqrt{\rho}\mathbb{E}\left[\mathbf{v}_k^H(\sqrt{\eta_{k,c}}\hat{\mathbf{v}}_k+\sqrt{\eta_{k,s}}\mathbf{u})\right] \quad (53)$$
$$=\sqrt{\eta_{k,c}\rho}\mathbb{E}\left[(\hat{\mathbf{v}}_k+\boldsymbol{\epsilon}_k)^H\hat{\mathbf{v}}_k\right]=\sqrt{\eta_{k,c}\rho}\mathbb{E}\left[\hat{\mathbf{v}}_k^H\hat{\mathbf{v}}_k\right]=\sqrt{\eta_{k,c}\rho}\mathrm{Tr}(\mathbf{C}_{\hat{v}_k}),$$

The term $DU_k$ in (23) is derived as

$$DU_k=\rho\mathbb{E}\left[\left|\mathbf{v}_k^H\mathbf{w}_kx_k-\mathbb{E}\left[\mathbf{v}_k^H\mathbf{w}_kx_k\right]\right|^2\right]=\rho\mathbb{E}\left[\left|\mathbf{v}_k^H\mathbf{w}_k\right|^2\right]-|DS_k|^2$$
$$=\rho\mathbb{E}\left[\left|\mathbf{v}_k^H(\sqrt{\eta_{k,c}}\hat{\mathbf{v}}_k+\sqrt{\eta_{k,s}}\mathbf{u})\right|^2\right]-|DS_k|^2=\eta_{k,c}\rho\xi\mathbb{E}\left[\left|\mathbf{v}_k^H\mathbf{C}_k\mathbf{v}_k\right|^2\right]$$
$$+\eta_{k,c}\rho\mathrm{Tr}\left(\mathbf{C}_{v_k}\mathbf{C}_k\mathbf{C}_k^H\right)+\eta_{k,s}\rho\mathrm{Tr}\left(\mathbf{C}_{v_k}\mathbf{u}\mathbf{u}^H\right)-|DS_k|^2, \quad (54)$$

where $\mathbf{C}_k=\mathbf{C}_{v_k\tilde{y}_k}\mathbf{C}_{\tilde{y}_k\tilde{y}_k}^{-1}$, and $\mathbb{E}[|\mathbf{v}_k^H\mathbf{C}_k\mathbf{v}_k|^2]$ in (54) can be expanded as (55). By evaluating (55) via [19, Lemma 7-9], (54) is written as (25). The term $IUI_{kj}$ in (24) is derived as

$$IUI_{kj}=\mathbb{E}\left[\left|\sqrt{\rho}\mathbf{v}_k^H\mathbf{w}_jx_j\right|^2\right]=\rho\mathbb{E}\left[\left|\mathbf{v}_k^H(\sqrt{\eta_{j,c}}\hat{\mathbf{v}}_j+\sqrt{\eta_{j,s}}\mathbf{u})\right|^2\right]$$
$$=\eta_{j,c}\rho\mathbb{E}\left[\left|\mathbf{v}_k^H\hat{\mathbf{v}}_j\right|^2\right]+\eta_{j,s}\rho\mathbb{E}\left[\left|\mathbf{v}_k^H\mathbf{u}\right|^2\right]=\eta_{j,c}\rho\xi\mathbb{E}\left[\left|\mathbf{v}_k^H\mathbf{C}_j\mathbf{v}_j\right|^2\right]$$
$$+\eta_{j,c}\rho\mathrm{Tr}\left(\mathbf{C}_{v_k}\mathbf{C}_j\mathbf{C}_j^H\right)+\eta_{j,s}\rho\mathrm{Tr}\left(\mathbf{C}_{v_k}\mathbf{u}\mathbf{u}^H\right), \quad (56)$$

where $\mathbf{C}_j=\mathbf{C}_{v_j\tilde{y}_j}\mathbf{C}_{\tilde{y}_j\tilde{y}_j}^{-1}$. Here, $\mathbb{E}[|\mathbf{v}_k^H\mathbf{C}_j\mathbf{v}_j|^2]$ in (56) can be evaluated as (57). By evaluating (57) via [19, Lemmas 7-9], the derivation can be completed as in (26).

## Appendix C
## Derivation of $\gamma$ in (28)

By denoting $\hat{\mathbf{V}}=[\hat{\mathbf{v}}_1,...,\hat{\mathbf{v}}_k,...,\hat{\mathbf{v}}_K]\in\mathbb{C}^{M\times K}$, $\boldsymbol{\Omega}=\mathrm{diag}(\sqrt{\eta_{1,c}},...,\sqrt{\eta_{k,c}},...,\sqrt{\eta_{K,c}})\in\mathbb{C}^{K\times K}$, and $\boldsymbol{\omega}=[\sqrt{\eta_{1,s}},...,\sqrt{\eta_{k,s}},...,\sqrt{\eta_{K,s}}]^T\in\mathbb{C}^K$, $\mathbf{W}$ in (18) is given by

$$\mathbf{W}=\hat{\mathbf{V}}\boldsymbol{\Omega}+\mathbf{u}\boldsymbol{\omega}^T. \quad (58)$$

From (29) and (58), the term $\mathbb{E}\left[|DE|^2\right]$ in (28) is derived as

$$\mathbb{E}\left[|DE|^2\right]=\mathbb{E}\left[\left|\sqrt{\rho}\mathbf{u}^H\mathbf{u}\mathbf{u}^H\mathbf{W}\mathbf{x}\right|^2\right]$$
$$=\rho\mathrm{Tr}\left(\mathbf{u}\mathbf{u}^H\right)^2\left(\mathbf{u}^H\mathbb{E}\left[\hat{\mathbf{V}}\boldsymbol{\Omega}\boldsymbol{\Omega}^H\hat{\mathbf{V}}^H\right]\mathbf{u}+\mathrm{Tr}\left(\mathbf{u}\mathbf{u}^H\right)^2\boldsymbol{\omega}^T\boldsymbol{\omega}\right)$$
$$=\rho\mathrm{Tr}\left(\mathbf{u}\mathbf{u}^H\right)^2\sum_{k=1}^{K}\left(\eta_{k,c}\mathbf{u}^H\mathbf{C}_{\hat{v}_k}\mathbf{u}+\eta_{k,s}\mathrm{Tr}\left(\mathbf{u}\mathbf{u}^H\right)^2\right). \quad (59)$$

## References


[1] H. Tataria *et al.*, "6G Wireless Systems: Vision, Requirements, Challenges, Insights, and Opportunities," *Proc. IEEE*, vol. 109, no. 7, pp. 1166–1199, 2021.

[2] F. Liu *et al.*, "Integrated Sensing and Communications: Toward Dual-Functional Wireless Networks for 6G and Beyond," *IEEE J. Sel. Areas Commun.*, vol. 40, no. 6, pp. 1728–1767, 2022.

[3] R. Liu *et al.*, "Joint Transmit Waveform and Passive Beamforming Design for RIS-Aided DFRC Systems," *IEEE J. Sel. Areas Commun.*, vol. 16, no. 5, pp. 995–1010, 2022.

[4] K. Zhong *et al.*, "Joint Waveform and Beamforming Design for RIS-Aided ISAC Systems," *IEEE Signal Process. Lett.*, vol. 30, pp. 165–169, 2023.

[5] Z. Yu *et al.*, "Active RIS Aided ISAC Systems: Beamforming Design and Performance Analysis," *IEEE Trans. Commun.*, 2023.

[6] X. Zhao *et al.*, "Dual-Functional MIMO Beamforming Optimization for RIS-Aided Integrated Sensing and Communication," *IEEE Trans. Commun.*, 2024.

[7] Z. Zhang *et al.*, "Intelligent Omni Surfaces Assisted Integrated Multi-Target Sensing and Multi-User MIMO Communications," *IEEE Trans. Commun.*, 2024.

[8] T. L. Marzetta *et al.*, *Fundamentals of Massive MIMO*. Cambridge University Press, 2016.

[9] Q. Wu *et al.*, "Intelligent Reflecting Surface-Aided Wireless Communications: A Tutorial," *IEEE Trans. Commun.*, vol. 69, no. 5, pp. 3313–3351, 2021.

[10] Q. Zhang *et al.*, "Power Scaling of Uplink Massive MIMO Systems with Arbitrary-Rank Channel Means," *IEEE J. Sel. Topics Signal Process.*, vol. 8, no. 5, pp. 966–981, 2014.

[11] E. Björnson and L. Sanguinetti, "Rayleigh Fading Modeling and Channel Hardening for Reconfigurable Intelligent Surfaces," *IEEE Wireless Commun. Lett.*, vol. 10, no. 4, pp. 830–834, 2020.

[12] J. Li and P. Stoica, *MIMO Radar Signal Processing*. John Wiley & Sons, 2008.

[13] S. M. Kay, *Fundamentals of Statistical Signal Processing: Estimation Theory*. Upper Saddle River, NJ, USA: Prentice-Hall, Inc., 1993.

[14] D. Gunasinghe and G. A. Aruma Baduge, "Achievable Rate Analysis for Multi-Cell RIS-Aided Massive MIMO with Statistical CSI-Based Optimizations," *IEEE Trans. Wireless Commun.*, vol. 23, no. 8, pp. 8117–8135, 2024.

[15] S. Boyd and L. Vandenberghe, *Convex Optimization*. Cambridge University Press, New York, NY, US, 2004.

[16] R. M. Fukuda and T. Abrão, "Linear, Quadratic, and Semidefinite Programming Massive MIMO Detectors: Reliability and Complexity," *IEEE Access*, vol. 7, pp. 29 506–29 519, 2019.

[17] R. Schmidt, "Multiple Emitter Location and Signal Parameter Estimation," *IEEE Trans. Antennas Propag.*, vol. 34, no. 3, pp. 276–280, 1986.

[18] 3GPP, "Technical Specification Group Radio Access Network; Spatial Channel Model for Multiple Input Multiple Output (MIMO) Simulations (Rrelease 17)," *TR 25.996*, 2022.

[19] T. V. Chien and H. Q. Ngo, "Massive MIMO Channels," in *Antenna and Propagation for 5G and Beyond*. IET Publishers, 2020.